Inorganic Chemistry

Article

pubs.acs.org/IC

# Apparent Anti-Woodward–Hoffmann Addition to a Nickel Bis(dithiolene) Complex: The Reaction Mechanism Involves Reduced, Dimetallic Intermediates

Li Dang,[†] Mohamed F. Shibl,[‡,∥] Xinzheng Yang,[†,¶] Daniel J. Harrison,[§,⊥] Aiman Alak,[§] Alan J. Lough,[⊥] Ulrich Fekl,*[,§,⊥] Edward N. Brothers,*[,‡] and Michael B. Hall*[,†]

[†]Department of Chemistry, Texas A&M University, College Station, Texas, U.S.A.

[‡]Science Program, Texas A&M University at Qatar, Doha, Qatar

[§]Department of Chemical and Physical Sciences, University of Toronto, Mississauga, Ontario, Canada L5L 1C6

[⊥]Department of Chemistry, University of Toronto, Toronto, Ontario, Canada M5S 3H6

Supporting Information

**ABSTRACT:** Nickel dithiolene complexes have been proposed as electrocatalysts for alkene purification. Recent studies of the ligand-based reactions of $Ni(tfd)_2$ (tfd = $S_2C_2(CF_3)_2$) and its anion $[Ni(tfd)_2]^-$ with alkenes (ethylene and 1-hexene) showed that in the absence of the anion, the reaction proceeds most rapidly to form the intraligand adduct, which decomposes by releasing a substituted dihydrodithiin. However, the presence of the anion increases the rate of formation of the stable *cis*-interligand adduct, and decreases the rate of dihydrodithiin formation and decomposition. In spite of both computational and experimental studies, the mechanism, especially the role of the anion, remained somewhat elusive. We are now providing a combined experimental and computational study that addresses the mechanism and explains the role of the anion. A kinetic study (global analysis) for the reaction of 1-hexene is reported, which supports the following mechanism: (1) reversible intraligand addition, (2) oxidation of the intraligand addition product prior to decomposition, and (3) interligand adduct formation catalyzed by $Ni(tfd)_2^-$. Density functional theory (DFT) calculations were performed on the $Ni(tfd)_2/Ni(tfd)_2^-$/ethylene system to shed light on the selectivity of adduct formation in the absence of anion and on the mechanism in which $Ni(tfd)_2^-$ shifts the reaction from intraligand addition to interligand addition. Computational results show that in the neutral system the free energy of activation for intraligand addition is lower than that for interligand addition, in agreement with the experimental results. The computations predict that the anion enhances the rate of the cis-interligand adduct formation by forming a dimetallic complex with the neutral complex. The $[(Ni(tfd)_2)_2]^-$ dimetallic complex then coordinates ethylene and isomerizes to form a Ni,S-bound ethylene complex, which then rapidly isomerizes to the stable interligand adduct but not to the intraligand adduct. Thus, the anion catalyzes the formation of the interligand adduct. Significant experimental evidence for dimetallic species derived from nickel bis(dithiolene) complexes has been found. ESI-MS data indicate the presence of a $[(Ni(tfd)_2)_2]^-$ dimetallic complex as the acetonitrile adduct. A charge-neutral association complex of $Ni(tfd)_2$ with the ethylene adduct of $Ni(tfd)_2$ has been crystallographically characterized. Despite the small driving force for the reversible association, very major structural reorganization (square-planar → octahedral) occurs.

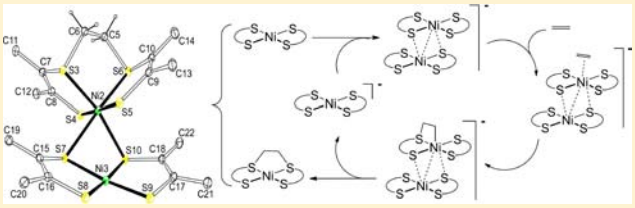

## INTRODUCTION

Olefin (alkene) purification is an important process in modern chemical industry, because organic feedstocks are largely olefin-based.[1] The traditional method, cryogenic distillation, is energy-intensive and expensive.[2] Approaches based on chemical reactions of olefins with metal salts such as copper are more efficient, but these metal salts are poisoned and deactivated by common olefin impurities, such as CO, $H_2S$, and acetylene.[3] Several studies, which include X-ray crystallographic characterization of cis-interligand adducts, reported that dithiolene complexes have high reactivity toward strained and cyclic alkenes (such as norbornadiene).[4−6] In 2001, Wang and Stiefel proposed that the nickel bis(dithiolene) complexes $Ni(S_2C_2(R)_2)_2$ (R = $CF_3$, CN) can be used to purify simple (terminal, noncyclic) olefins by reacting with the olefin (and not its common impurities) to produce the interligand product, which upon reduction releases the pure olefin.[7] This reaction was proposed to involve four steps (Scheme 1): (1) the monoanionic complex $[NiL_2]^-$ (L = dithiolene, such as mnt ($S_2C_2(CN)_2$) or as in the current study tfd ($S_2C_2(CF_3)_2$)) is oxidized electrochemically to the neutral species $[NiL_2]$; (2) $[NiL_2]$ selectively binds the olefin, forming the adduct $[(olefin)NiL_2]$; (3) the olefin adduct is electrochemically

**Received:** October 12, 2012
**Published:** March 13, 2013

   dx.doi.org/10.1021/ic302236u | *Inorg. Chem.* 2013, 52, 3711−3723

**Scheme 1**

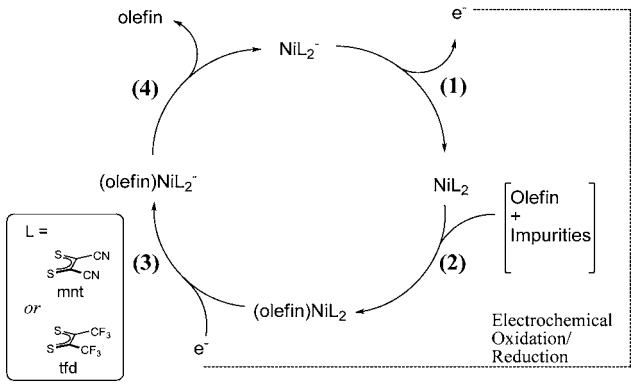


reduced, generating $[(\text{olefin})\text{NiL}_2]^-$; and (4) the reduced olefin adduct $[(\text{olefin})\text{NiL}_2]^-$, rapidly ejects the olefin, thus regenerating $[\text{NiL}_2]^-$. The cis-interligand adduct, where two sulfurs of different dithiolene ligands are bridged by a new two-carbon bridge, was thought to be formed in step 2.[7] Previous X-ray crystallography confirmed such a structure (for norbornadiene and $\text{Ni}(\text{S}_2\text{C}_2(\text{CF}_3)_2)_2$).[6b] After this X-ray structure report, it was often assumed that *inter*ligand addition is the main reaction, with a side reaction being the *intra*ligand addition, that is, where the alkene has added to two sulfurs in the same ligand (see Scheme 3 below). However, such a selectivity would be in contradiction to orbital symmetry considerations, which predict that formation of the cis-interligand adduct is symmetry-forbidden, whereas the formation of the intraligand adduct is symmetry-allowed.[5a,b,8] A previous theoretical study showed that a direct (without the anion) reaction for the formation of the cis-interligand adduct could avoid the constraints imposed by orbital symmetry if it is a two-step process, in which a twisted (pseudotetrahedral) adduct forms and then isomerizes to the more thermodynamically stable square-planar cis-interligand product (Scheme 2).[8]

The use of electron-withdrawing groups on the dithiolene, such as cyano (mnt) or trifluoromethyl (tfd), not only significantly lowers the activation energy for the adduct formation, but it also strongly stabilizes the products. However, these substituents leave the free energy of activation for the conformational transformation nearly unchanged.[8] The electronic structure of nickel dithiolenes has been studied by theoretical methods[9] and various spectroscopies.[10] Applications of alkene reactions of dithiolenes[11] have been extended to molybdenum tris(dithiolenes)[12] and to platinum bis(dithiolenes) with 1,4-dienes.[13] New theoretical studies directly addressed the alkene binding mechanism for square-planar bis(dithiolenes) and simple alkenes, but were limited to charge-neutral species.[14] Some kinetic studies on the mechanism of the reaction of nickel dithiolene with alkenes were previously reported.[4c,7] However, the initial mechanistic work on square-planar bis(dithiolenes) and monoolefins has to be regarded incomplete, because a key experimental finding from 2006 has not been addressed either by detailed kinetics or computations; namely, that it was conclusively demonstrated for $\text{Ni}(\text{S}_2\text{C}_2(\text{CF}_3)_2)$ ($\text{Ni}(\text{tfd})_2$, compound **1**) that the one-electron-reduced form of the metal complex is crucially involved.[15] In the presence of the reduced reactant $[\text{Ni}(\text{tfd})_2]^-$ ($\mathbf{1}^-$), the cis-interligand adduct **2** was observed as the main product of the reaction of **1** with ethylene (Scheme 3, bottom, R = H). However, the intraligand adduct **3** is formed and its decomposition product, substituted dihydrodithiin (**DHD**), is observed in the absence of $\mathbf{1}^-$, which can be achieved with rigorously purified material (Scheme 3, top). Analogous observations were made for 1-hexene (Scheme 3, R = $^n$Bu; products are **2′** or **3′** + **DHD′**).[15]

Although a mechanism was proposed, it was based on mostly qualitative observations; neither was a full mechanism fitted to kinetic data nor were computational data involving the anion available. We now report here a combined experimental (kinetics) and computational (density functional theory, DFT) study to provide much deeper insight into the mechanism.[16] The experimental work involves global analysis kinetics for the case of 1-hexene, using a multitude of time traces that were fitted simultaneously. The computational work investigates the possible pathways leading to different addition products as shown in Scheme 3. DFT computations were carried out for the intermediates and transition states for the reactions of $\text{Ni}(\text{tfd})_2$ (**1**) and its anion ($\mathbf{1}^-$) with ethylene. Computations thus elucidate the role of $[\text{Ni}(\text{tfd})_2]^-$ ($\mathbf{1}^-$), which appears to control the selectivity for different products, uncovering an important new mechanism that is consistent with the experimental results.

## RESULTS AND DISCUSSION

1-Hexene was chosen for the experimental work because it is a liquid, and ethylene was chosen for the computational work because it makes the size of the system more feasible.

**Experimental Results and Stoichiometric Mechanism.** Pure $\text{Ni}(\text{tfd})_2$ (**1**, Scheme 3) reacts with 1-hexene to produce mostly a substituted dihydrodithiin (**DHD′**), via the short-lived (not directly observed) intraligand addition product **3′**,[17] along with small amounts of a stable interligand adduct of the alkene (**2′**).[18] The presence of the reduced metal complex ($\mathbf{1}^-$) changes the product selectivity from preferred **DHD′**-formation to preferred **2′**-formation (Scheme 3). We have obtained 24 time traces, stemming from 8 different kinetic runs where $\mathbf{1}^-$ and 1-hexene (**hex**) concentrations were varied. All reactions were at 298 K in $\text{CDCl}_3$. In each run, the concentrations of the three directly observable (long-lived and NMR-active) species **1**, **DHD′**, and **2′** were independently

**Scheme 2**

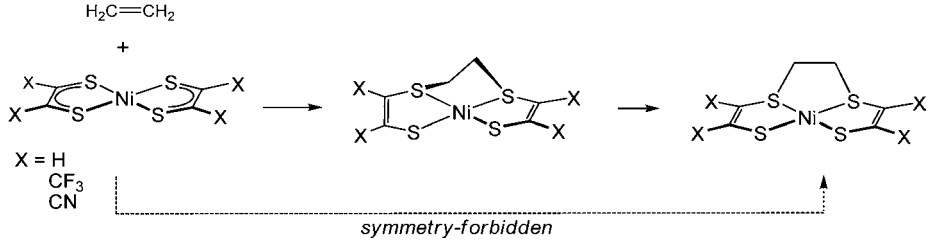



dx.doi.org/10.1021/ic302236u | Inorg. Chem. 2013, 52, 3711−3723

**Scheme 3**

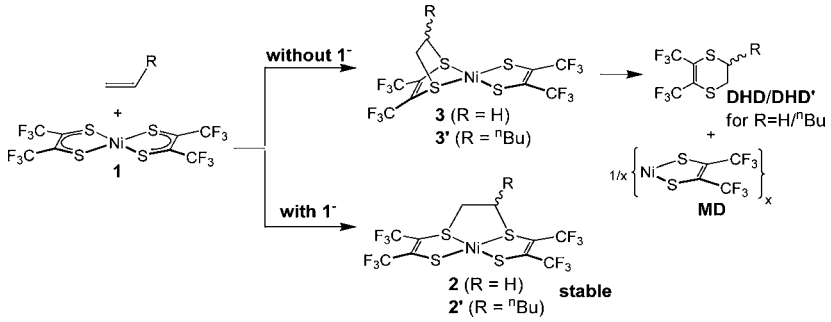


monitored by $^{19}$F-NMR. Each time trace contains typically 15−20 data points. All 24 time traces (459 data points) were fitted, simultaneously and globally, to various models, using the DynaFit[19] (version 3.28) program. The parameters to be determined are globally optimized using all (459) data points available. This is a more rigorous approach than fitting each time trace individually. The best fit (Figure 1; see below for assessment of fit quality) was obtained for the "parallel reactions" model shown in Scheme 4.

The largest known source of error in this kinetic study is the error from manual integration of NMR intensities, leading mostly to statistical scatter but most probably to some small systematic deviations as well.[20] The overall quality of the fit

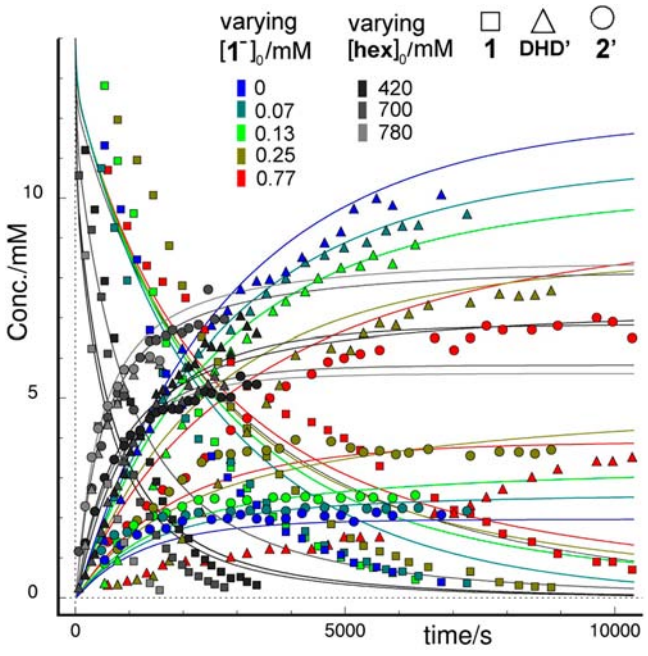


**Figure 1.** Kinetic analysis: Global analysis fit (solid curves) of the model in Scheme 4 to the set of 24 time-traces for **1** (squares), **DHD′** (triangles) and **2′** (circles), using different starting concentrations $[\mathbf{1}^-]_0$ and $[\mathbf{hex}]_0$ at 298 K in CDCl3. $[\mathbf{1}]_0$ was between 13.2 and 14.0 mM (exact values in the Supporting Information). Where $[\mathbf{1}^-]_0$ was varied (data points in color), $[\mathbf{hex}]_0$ was 140 mM. For $[\mathbf{1}^-]_0$ = 0, a value of $1 \times 10^{-6}$ mM was used as in lieu of exactly zero, to avoid "division by zero" error. For experiments where $[\mathbf{hex}]_0$ was varied (data points in shades of gray), $[\mathbf{1}^-]_0$ was 0.25 mM. Plots where each experimental time trace is individually compared to its predicted time trace (24 plots) are available in the Supporting Information. Rate constants and equilibrium constant $K_{ox}$ are obtained from the fit and are reported in Table 1.

**Scheme 4**

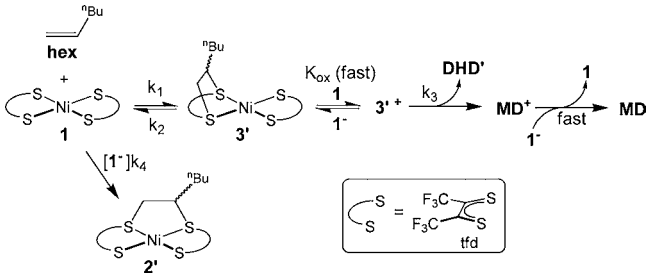


(Figure 1) to the model in Scheme 4 appears visually very acceptable, considering how it reproduces the concentration dependence for [**hex**], the slight slowing down of the decay of **1** in the presence of $\mathbf{1}^-$, and, most importantly, the hard-to-understand changeover in selectivity from **3′** production (**DHD′** is observed) to **2′** production in the presence of $\mathbf{1}^-$.

Despite some imperfections that are noted,[20] this model is superior to all other models we tried. Our assessment is based on Akaike's rigorous quantitative method as implemented in Dynafit.[19] It is often difficult to reliably assign a correct reaction mechanism and to rule out competing mechanisms if the data contain noise and if the mechanisms considered are all fairly complex, as is the case here. In particular, if the quality of a fit is assessed solely based on the resulting squared deviations between fitted curve and experimental data points, the danger of "overfitting" arises: more complicated models that have more parameters than competing simpler models seem to fit better, simply because they add more degrees of freedom to the fitting procedure, even if parameters in the fit to the more complicated model are not physically/chemically meaningful. Therefore, we chose to use a model discrimination analysis using Akaike's method (corrected Akaike Information Criterion, AICc).[21] This method arises from an information theoretical approach to ranking of competing models: it has an inbuilt tendency to balance simplicity of a model and goodness of fit. In essence, a model will be penalized not only for poor fit but also for increased number of parameters, such that overfitting is avoided and comparison is possible across models having different numbers of parameters. An AICc value for a model that uses experimental input data is derived from the AIC value (Akaike information criterion). The AIC is defined as $2K - 2\log(\text{likelihood})$ (with $K$ = number of parameters, likelihood in a statistical sense meaning quality of fit). The AIC$_c$ value is the AIC value multiplied by a correction factor that becomes significantly different from unity only for small data sets and which assures that Akaike's method is correct for small data sets as well. Since AIC and AICc become virtually identical for large


dx.doi.org/10.1021/ic302236u | Inorg. Chem. 2013, 52, 3711−3723

data sets, it is generallly recommended to use the AICc for all data sets, large and small.[21] The "parallel reactions" model (Scheme 4, fit in Figure 1) wins, against all other models we tried, by a wide margin. The second and third best models we found are isomerization models, in which branching is proposed to occur from the common intermediate **3′**. In such a proposed mechanism, **3′** would decompose in the absence of $\mathbf{1}^-$ (to form **DHD′** and **MD**), but, if $\mathbf{1}^-$ catalyst is present, **3′** isomerizes to form **2′**. Both a basic three parameter isomerization model and a more sophisticated 5-parameter isomerization model (reversibility in the initial addition to form **3′** and postulation of an unobservable intermediate before decomposition of **3′**; see Supporting Information) provide fits that are objectively inferior compared to the "parallel reactions" model described in Scheme 4. This assessment (objectively inferior) is made based on Akaike's method: our second best model is the 5-parameter isomerization model (coincidently the same number of free parameters as the model in Scheme 4) that compares already very unfavorably. AICc values are used as the deciding criterion. A higher AICc value of a competing model correspond to less empirical support compared to the better model, where the numerical difference, Δ, in AICc of the model compared to the higher ranked model is taken as the indicator. A Δ between 4 and 7 is generally interpreted as "considerably less" empirical support for the contender model, and a Δ of larger than 10 is customarily seen as "essentially no empirical support" for the contender model (using the terminology of the field). The 5-parameter isomerization model is associated with Δ = 95 compared to the model in Scheme 4. The three-parameter isomerization model fares even less well in a direct comparison with the model in Scheme 4 (Δ = 156), such that the runner-up models receive essentially no empricial support compared to the model in Scheme 4, which can be fairly stated to be the best model we found. While Akaike's method provides only a relative ranking and no absolute confirmation of a model (the theoretical possibility remains that a yet to be discovered model ranks even higher than Scheme 4), we find the *combined* evidence from data fitting *and* quantum chemistry (see below) rather convincing.

The "parallel reactions" model (Scheme 4) is not only favored on kinetic grounds but is also judged chemically reasonable. It is highly realistic that the intraligand addition step is reversible (second-order $k_1$, first-order $k_2$). Reversible alkene addition[11] to form an intraligand adduct has been observed for a *molybdenum tris*(dithiolene) complex.[12a] The oxidation of the intraligand adduct **3′** to form a cationic species ($K_{ox}$) is judged to be reasonable, considering that **3′** contains a true ene-1,2-dithiolate. Ene-1,2-dithiolate-containing model complexes, nitrogen-chelated compounds $(\hat{N}N)Ni(S_2C_2(CF_3)_2)$, are oxidized to their cations at potentials that are very similar to the redox potential for $\mathbf{1}/\mathbf{1}^-$.[22] Regarding the decomposition step: since ligand substitution at square-planar nickel(II) is typically associative,[23] it is reasonable to expect that the cationic species will be more labile, and **DHD′** is lost through ligand substitution. Regarding the final electron transfer step: polymeric/oligomeric metal decomposition products were observed by NMR spectroscopy, and the simplifying assumption is made in the model that $\mathbf{MD}^+$ gets completely reduced by $\mathbf{1}^-$ to rapidly regenerate **1**. Somewhat incomplete reduction, however, would be an excellent explanation for Geiger's observation[4e] that small amounts of $\mathbf{1}^-$ are produced in the reaction of neutral **1** with norbornadiene. For **2′** formation, we modeled a step that is overall third order: first order in **1**, first order in $\mathbf{1}^-$, first order in hexene.[24] $\mathbf{1}^-$ is regenerated in this step, so $\mathbf{1}^-$ is a true catalyst. We are aware of the low likelihood that an actual trimolecular reaction occurs. However, a true trimolecular reaction is not a necessary requirement for a third order reaction: a third-order dependence can result if an association complex is formed reversibly (with a not too large equilibrium constant) between two species and if the association complex then reacts with the third species. It was previously suggested that $\mathbf{1}^-$ might bind 1-hexene to form $\mathbf{2}^-$, which then gets reoxidized by **1**.[15] The computational work reported here (below) suggests that the formation of $\mathbf{2}^-$ is prohibitively uphill, but a new sequence of reversible reactions was found that can lead to an overall third-order behavior (below, section Computational Results and Intimate Mechanism).

The analysis of kinetic data has yielded valuable experimental information on the stoichiometric mechanism. A mechanistic branching via isomerization at the level of the intraligand adduct (decomposition versus anion-catalyzed isomerization) can be ruled out with reasonable certainty. The model that fits the data best involves an $Ni(tfd)_2^-$ anion catalyzed formation of the stable interligand adduct. In a parallel pathway, the decomposition of a (reversibly formed) intraligand adduct is dependent on its prior oxidation. The anion concentration thus has a second role, since it affects the decomposition rate by effectively changing the redox potential in solution. Higher concentration of $\mathbf{1}^-$ shifts the oxidation reaction to the left such that decomposition is slowed down and interligand adduct can be formed since $\mathbf{1}^-$ catalyzes the formation of interligand adduct. It was found that $\mathbf{1}^-$ catalyzes **2′** formation in a step that depends on $k_4[\mathbf{1}][\mathbf{1}^-][\mathbf{hex}]$. While finding a stoichiometric mechanism is the strength of experimental kinetics, the ability to find structures of short-lived intermediates and transition states is clearly a strength of quantum chemistry. A mechanism detailing exactly how $\mathbf{1}^-$ catalyzes formation of stable adducts will emerge from the computational results discussed below. All kinetic parameters for the stoichiometric mechanism from experiment (Scheme 4, 5 free parameters; $k_1$ through $k_4$, $K_{ox}$) are reported in Table 1.

**Table 1. Numerical Results for Rate Constants and $K_{ox}$ Equilibrium (298 K in $CDCl_3$), from the Fit (Figure 1) to the Model Shown in Scheme 4**

| | |
|---|---|
| $k_1$ | $1.3(7) \times 10^{-5}$ $mM^{-1}$ $s^{-1}$ |
| $k_2$ | $5(4) \times 10^{-2}$ $s^{-1}$ |
| $K_{ox}$ | $5(2) \times 10^{-2}$ |
| $k_3$ | $9.5(8) \times 10^{-3}$ $s^{-1}$ |
| $k_4$ | $1.91(8) \times 10^{-6}$ $mM^{-2}$ $s^{-1}$ |

**Computational Results and Intimate Mechanism.** All computations involved the full tfd-system including $CF_3$ substitutents, as used experimentally. Ethylene can bind to the nickel bis(dithiolene) complexes **1** and $\mathbf{1}^-$ in a variety of ways as shown in Scheme 5. Five possible addition products were fully optimized as stable species (local minima): the cis-interligand adduct **2**($\mathbf{2}^-$), the twisted interligand adduct **2y**($\mathbf{2y}^-$), the intraligand adduct **3**($\mathbf{3}^-$), ethylene coordinated to nickel **4**($\mathbf{4}^-$), and the nickel−sulfur adduct **5**($\mathbf{5}^-$).

In the following, solvation corrected relative free energies in kcal/mol will be reported and discussed, unless otherwise noted. The relative free energies and relative electronic energies calculated with ω-B97XD/6-31++G** and relative electronic


dx.doi.org/10.1021/ic302236u | Inorg. Chem. 2013, 52, 3711−3723

**Scheme 5**

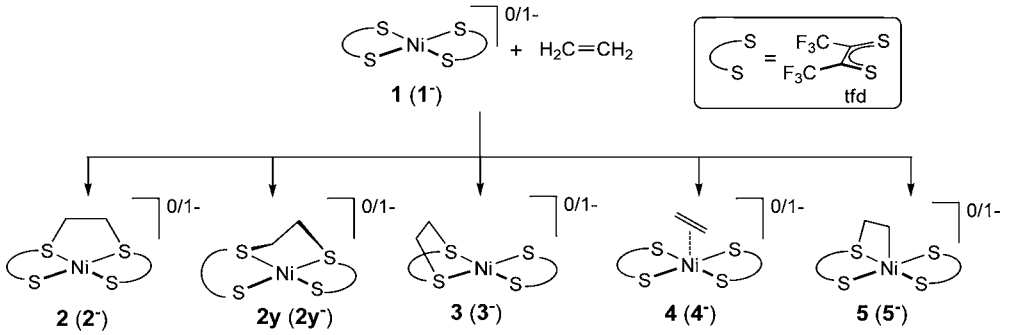


energies calculated with M06/6-31++G** (see Methods section below) will be given in the Supporting Information.

Figure 2 shows the calculated reaction pathways for the reaction of the neutral nickel bis(dithiolene) **1** with ethylene to give either the cis-interligand adduct (**2**) or the intraligand adduct (**3**) followed by dihydrodithiin (**DHD**) elimination and metal complex dimer (**MD**) formation. The gas-phase structural parameters of the species involved in Figure 1 (and other species discussed below) are shown in the Supporting Information. Calculated gas-phase geometrical parameters for **1** and **2** agree well with experimentally determined[25,15] values, thus confirming that the functional and basis sets are adequate for the structures. While the experimentally observed metal decomposition product displays a very large number of inequivalent fluorines in the $^{19}$F-NMR spectrum and is assigned as a mixture of many oligomers and polymers (reasonable, since monomeric Ni(tfd) is unstable), for the sake of simplicity, **MD** is modeled as a dimer only in the computations. The results show that cis-interligand adduct **2** can be formed via direct addition of **1** with ethylene, by overcoming a free energy of activation of 26.0 kcal/mol to form the twisted cis-interligand intermediate, **2y**, as shown in a previous communication.[8] Interligand addition is only symmetry-allowed if it goes via this twisted intermediate. This twisted cis-interligand intermediate, **2y**, then isomerizes to give the thermodynamically more stable cis-interligand **2** through a free energy of activation of 16.5 kcal/mol. However, consistent with the recent experimental results,[15] the free energy of activation for the formation of the intraligand adduct, **3**, is predicted to be lower than the rate-determined free energy of activation of the formation of **2** by 7.7 kcal/mol. The intraligand adduct, **3**, subsequently decomposes to **DHD** (observed) and **MD**.[15] Here, the DFT-computed free energy of activation for the formation of **3** (18.3 kcal/mol) is consistent with the free energy of activation calculated from rate constant $k_1$ in Table 1 (20.0(3) kcal/mol, using the Eyring–Polanyi equation), indicating that the computation is reliable, with less than 2 kcal/mol deviation from the experimental result in this case.

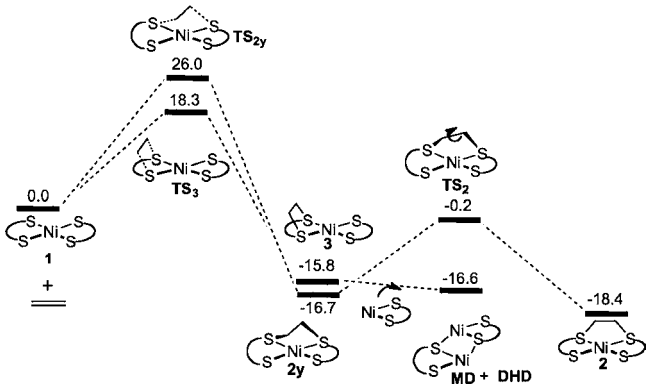


**Figure 2.** Free-energy profile for the reactions of **1** with ethylene to form interligand adducts **2y** and **2**, the intraligand adduct **3** and decomposition products **DHD**/**MD**. Relative free energies in solvent are given in kcal/mol.

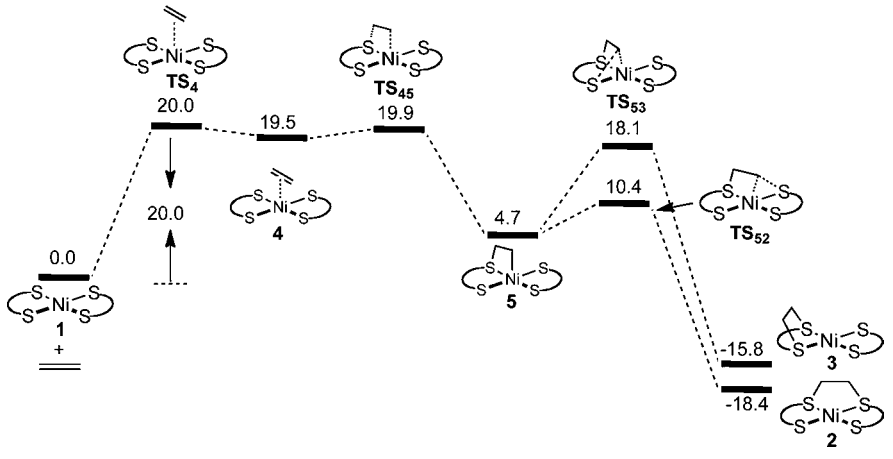


**Figure 3.** Free-energy profile for the alternative (initial metal-coordination) reaction pathways of **1** with ethylene to form interligand adduct **2** or intraligand adduct **3** via **4** and **5**. Relative free energies in solvent are given in kcal/mol.


dx.doi.org/10.1021/ic302236u | Inorg. Chem. 2013, 52, 3711−3723

Alternative reaction pathways to generate adducts **2** and **3** from neutral nickel bis(dithiolene) **1** and ethylene are shown in Figure 3. These pathways begin with the direct coordination of ethylene to Ni, forming intermediate **4**, which can isomerize to **5**, in which ethylene has added across a Ni−S bond, via transition state $\mathbf{TS}_{45}$. Then, **5** can isomerize into either **3** or **2** with free energies of activation of 13.4 and 5.7 kcal/mol, respectively. The more favorable route to the formation of **2** over **3**, found here, may be a key aspect of the mechanism. Since $\mathbf{TS}_4$, **4**, and $\mathbf{TS}_{45}$ are very similar in their free energy, one might expect to find a direct route from **1** and ethylene to **5**. In spite of several searches, an alternative transition state for the direct formation of **5** could not be found; when the $CH_2-CH_2$ fragment on **5** was moved away from the nickel sulfur bond, convergence to either $\mathbf{TS}_4$ or $\mathbf{TS}_{45}$ was always found rather than a direct transition state connecting **5** and the separated nickel bis(dithiolene) (**1**) and ethylene. However, a direct route leading to Ni−S bound intermediate was found for $Ni(mnt)_2$ (mnt = $S_2C_2(CN)_2$).[26] Although the reactions from intermediate **4** proceeds easily to the formation of **2**, the formation of **4** requires a free energy of activation of 20.0 kcal/mol, which although less than $\mathbf{TS}_{2y}$, is still larger than the free energy of activation for the direct formation of **3** from neutral nickel bis(dithiolene) **1** and ethylene (Figure 2). Therefore, formation of dihydrodithiin (**DHD**) through the intraligand intermediate **3** is the most favorable pathway in the neutral system, consistent with the experimental finding[15] that pure nickel bis(dithiolene) **1** reacts with alkenes to give substituted dihydrodithiins and decomposition products as the major route.

While it is clear why the decomposition pathway is favored, it is still necessary to elucidate one of the most surprising experimental findings: according to the qualitative[15] and quantitative (see above) experimental results, the presence of the anionic nickel bis(dithiolene) ($\mathbf{1}^-$) results in the formation of cis-interligand adduct **2** as the major product, rather than the formation of the unstable intraligand adduct **3**. One proposed possibility is direct concerted formation of $\mathbf{2}^-$ from $\mathbf{1}^-$ and ethylene and then electron transfer between $\mathbf{2}^-$ and **1** to give **2** and regenerate $\mathbf{1}^-$ (Scheme 6).[15] This suggestion does involve $\mathbf{1}^-$ as a catalyst in the formation of **2**, and its thermodynamic feasibility need to be examined computationally.

**Scheme 6**

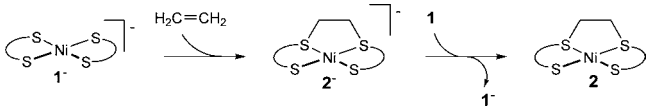


Computed reaction pathways for the reaction of anionic nickel bis(dithiolene) ($\mathbf{1}^-$) with ethylene are shown in Figure 4. The formation of interligand anion adducts $\mathbf{2y}^-$ and $\mathbf{2}^-$ follows a similar route to that of the neutral species as shown in Figure 1; however, the free energy of activation for the transformation of $\mathbf{1}^-$ and ethylene into interligand adduct $\mathbf{2y}^-$ is 43.9 kcal/mol, much higher than that of the neutral system. The route to $\mathbf{3}^-$ is somewhat more complicated than that to the neutral **3**, the former proceeds through two steps, with one S−C bond forming in each step (Figure 4b). Again, the free energy of activation for the intraligand adduct $\mathbf{3}^-$ is 44.1 kcal/mol (Figure 4b), much higher than that for **3** in neutral system (Figure 2). These high free energies of activation are in line with the instability of the anionic cis-interligand and intraligand adducts

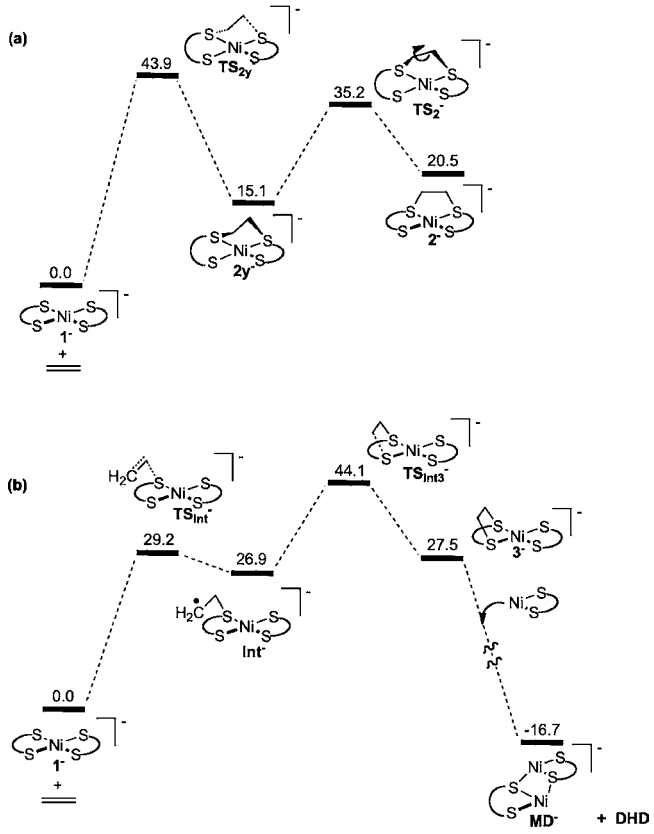


**Figure 4.** Free-energy profiles for (a) the reaction of anionic nickel bis(dithiolene) $\mathbf{1}^-$ with ethylene to form interligand adduct $\mathbf{2}^-$ and (b) the decomposition to product $\mathbf{MD}^-$ and **DHD** from intraligand adduct $\mathbf{3}^-$ via intermediate $\mathbf{Int}^-$. Relative free energies in solvent are given in kcal/mol.

$\mathbf{2}^-$ and $\mathbf{3}^-$, as $\mathbf{2}^-$ is the electrochemically produced species that regenerates $\mathbf{1}^-$ and ethylene in the original catalytic cycle. Although $\mathbf{2}^-$ and $\mathbf{3}^-$ can transfer an electron to **1**, thus giving $\mathbf{1}^-$ and the more stable **2** and **3**, neither $\mathbf{2}^-$ nor $\mathbf{3}^-$ will form rapidly enough to explain the experimental observation, suggesting that the free energies of activation for the proposed mechanism in Scheme 6 is too high, so another route must be found.

Figure 5a shows a route where the nickel bis(dithiolene) anion $\mathbf{1}^-$ first coordinates ethylene to form the anionic intermediate $\mathbf{4}^-$ (an alkene complex of nickel) through a transition state $\mathbf{TS}_4^-$ with a free energy of activation of 16.8 kcal/mol. Although the formation of $\mathbf{4}^-$ is viable, its reactions leading to $\mathbf{2}^-$ or $\mathbf{3}^-$ via intermediate $\mathbf{5}^-$ still have high free energies of activation. Attempts to locate the transition state from $\mathbf{4}^-$ to $\mathbf{5}^-$ failed and a potential energy scan from $\mathbf{5}^-$ along the Ni−C and S−C (ethylene fragment) bonds leads to the intermediate $\mathbf{Int}^-$ through $\mathbf{TS}_{\mathbf{Int\text{-}5}}^-$ (Figure 5b). Thus, the overall free energy of activation for forming $\mathbf{5}^-$ from $\mathbf{1}^-$ and $C_2H_4$ via the intermediate $\mathbf{Int}^-$ in Figure 5b is also high at 32.8 kcal/mol. Even though the transformation from $\mathbf{5}^-$ to $\mathbf{2}^-$ requires less energy than that from $\mathbf{5}^-$ to $\mathbf{3}^-$ (Figure 5a), the overall free energy of activation for the formation of $\mathbf{2}^-$ from $\mathbf{1}^-$ + $C_2H_4$ (Figure 5a) is still high at 37.1 kcal/mol. Therefore, this alternative route is also not able to compete kinetically with the formation of **3** from neutral $Ni(tfd)_2$ (**1**) and ethylene, which has a free energy of activation of 18.3 kcal/mol (Figure 2). It is worth noting that any mechanism for the formation of stable adducts that goes through $\mathbf{Int}^-$ is likely inconsistent with


dx.doi.org/10.1021/ic302236u | Inorg. Chem. 2013, 52, 3711−3723

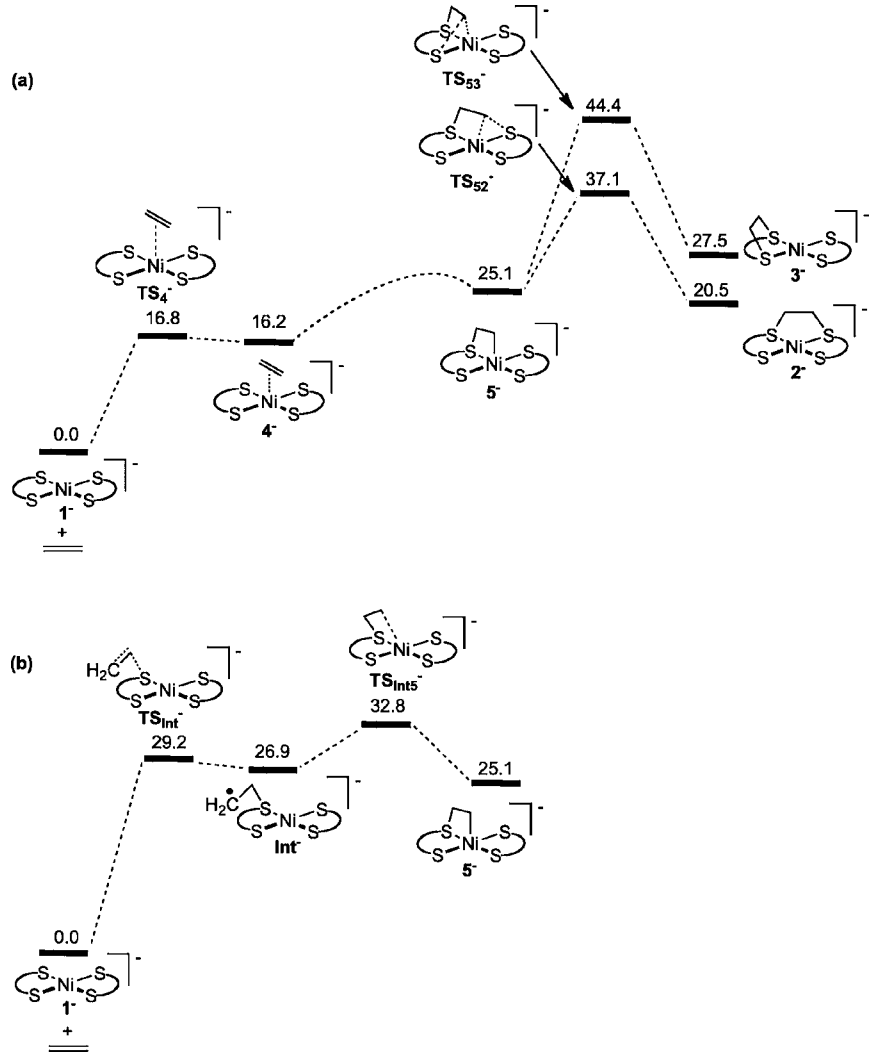


**Figure 5.** Free-energy profiles for (a) the other reaction pathways of $\mathbf{1}^-$ with ethylene to form cis-interligand adduct $\mathbf{2}^-$ or intraligand adduct $\mathbf{3}^-$ via formation of $\mathbf{4}^-$ and $\mathbf{5}^-$, (b) formation of $\mathbf{5}^-$ from $\mathbf{1}^-$ and ethylene via intermediate $\mathbf{Int}^-$. Relative free energies in solvent are given in kcal/mol.

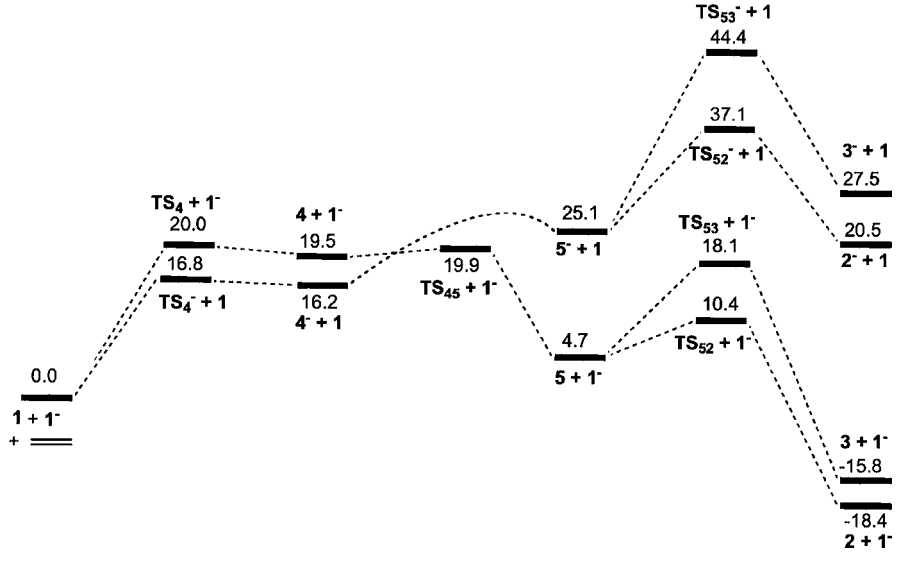


**Figure 6.** Free-energy profile (structures in Figure 3) for the reaction pathways of **1** and $\mathbf{1}^-$ with ethylene to form interligand adducts **2**($\mathbf{2}^-$) and intraligand adducts **3**($\mathbf{3}^-$) via intermediates **5**($\mathbf{5}^-$). Relative free energies in solvent are given in kcal/mol.


dx.doi.org/10.1021/ic302236u | *Inorg. Chem.* 2013, 52, 3711−3723

existing experimental stereochemistry (unless **Int**$^-$ collapses rapidly enough); for selectively deuterated 1-hexene, stereoretention,[15] which would be hard to reconcile with intermediate **Int**$^-$, was observed for the stable adduct (selectively deuterated **2′**).

The energies from Figures 3 and 5a are combined in Figure 6 simply by referencing the energy to **1** + **1**$^-$ + $C_2H_4$. Here, one can see how adduct **2** might form through a pathway with a low free energy of activation in the presence of anion **1**$^-$. The anion could catalyze the reaction indirectly through the formation of **4**$^-$, which transfers an electron to **1** as it forms **5** on the neutral potential energy surface via a transition state $\mathbf{TS_{45}}$ followed by an isomerization of **5** to **2** as discussed above. Unfortunately, both **4** and $\mathbf{TS_{45}}$ are higher in free energy than the transition state for the formation of **3** directly from **1** and ethylene.

The discussion to this point has focused primarily on precluding various reaction routes, but an explanation for how **1**$^-$ catalyzes the production of **2** has not been offered so far. All reactions of **1**$^-$ with ethylene considered to this point lead to high free energies of activation and unstable products. However, if a low energy route to **5** exists, species **5** easily isomerizes to **2** and not **3** through a low free energy of activation (Figure 3). Having exhausted possible steps for either of the monomers **1** or **1**$^-$ to lead independently to a viable route, we calculated the dimetallic complex formed from **1** + **1**$^-$. Formation of this dimetallic complex, **D0**$^-$, is surprisingly favorable (Figure 7) with an enthalpy of binding in solution of

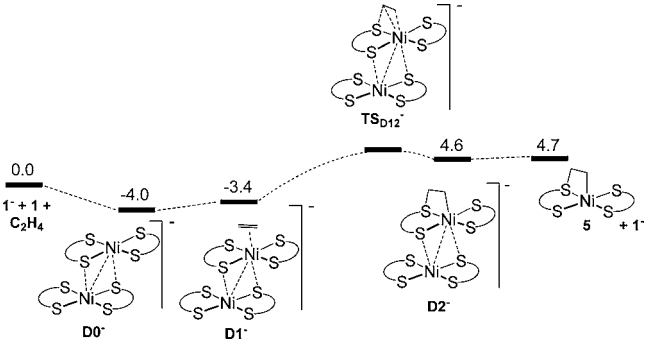


**Figure 7.** Free-energy profiles for formation of **5** and **1**$^-$ via **D0**$^-$, **D1**$^-$, and **D2**$^-$. For $\mathbf{TS_{D12}}^-$, a relaxed potential energy surface (PES) scan from **D2**$^-$, along the Ni−C and S−C distance, shows that the PES is flat from **D2**$^-$ to $\mathbf{TS_{D12}}^-$. Relative free energies, in solvent, are given in kcal/mol. Species **5** easily transforms into stable interligand adduct **2** as shown in Figure 3.

−21.8 kcal/mol (free energy of binding in solution equal to −4.0 kcal/mol). This stable **D0**$^-$ can react with ethylene to give **D1**$^-$; then, **5** and **1**$^-$ will be formed via **D2**$^-$ through a transition state $\mathbf{TS_{D12}}^-$ (Figure 7). The initial product **5** is readily transformed into **2** rather than **3** as shown in Figure 3. The reaction leading to the formation of **5** via this dimetallic species seems to be the most likely way for **1**$^-$ to act as a catalyst for the production of **2** as free energies of activation for the formation of **2**$^-$ from **1**$^-$ are too high. None of the other reaction pathways can compete with this process of forming **2** via **5** as shown in Figures 3 and 7.

The stability of **D0**$^-$ can be explained by examining the interaction of the frontier molecule orbitals (MOs) of two monomers, **1**. The molecular orbitals of **1** have been discussed previously.[27] In Figure 8 the highest occupied MO (HOMO) and the lowest unoccupied MO (LUMO) of **1** interact

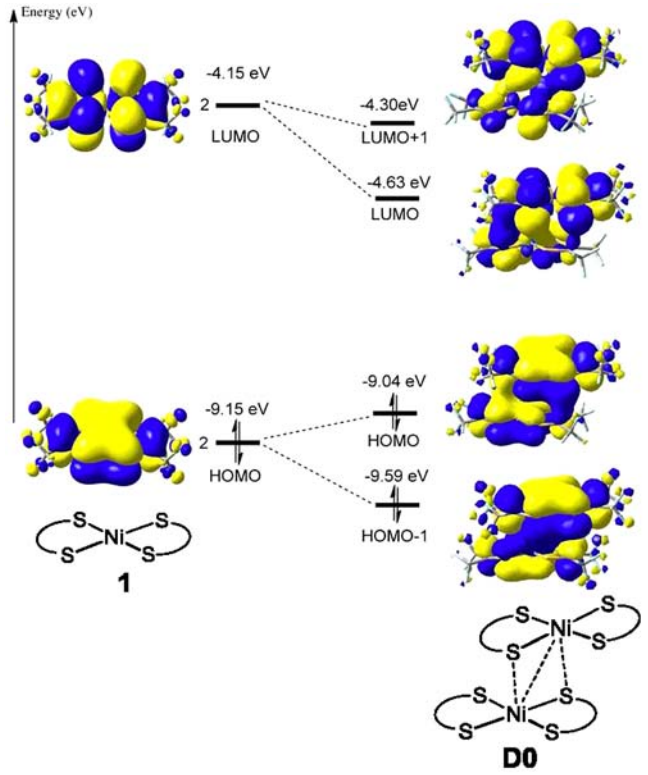


**Figure 8.** Interactions of the frontier molecular orbitals in **1** are shown for **D0**, the neutral analog of **D0**$^-$ in Figure 7, in the geometry of **D0**$^-$. The high stability of **D0**$^-$ arises from the additional electron in the strongly stabilized LUMO of **D0**.

primarily with each other to form the HOMO and HOMO−1, LUMO and LUMO+1 of the dimer, respectively. Note that for HOMO interactions the in-phase (bonding) combination is stabilized more than the out-of-phase (antibonding) combination. For LUMO interactions, both the in-phase (bonding) combination and the out-of-phase (bonding) combination are stabilized because of the "slipped" geometry. Although the neutral dimer is weakly stabilized by this slipped interaction, placing one electron in the LUMO of the dimer (Figure 8) to form **D0**$^-$ strongly stabilizes this anionic dimetallic complex. The formation of the stable **D0**$^-$ as shown in Figure 7 is the key process by which **1**$^-$ catalyzes production of **2**, a prediction consistent with the experimental result that high **1**$^-$ concentrations are needed to favor the interligand alkene adducts over decomposition products.[15]

Although the binding of the alkene to **D0**$^-$ to form the initial alkene adduct (**D1**$^-$) is weak (Figure 7), this intermediate is much more favorable than alkene binding to either **1** or **1**$^-$ in the formation in **4** or **4**$^-$. Subsequently, the transition between the initial adduct, **D1**$^-$, and the species with the alkene added across the Ni−S bond (**D2**$^-$) occurs on an extremely flat potential energy surface. Numerous attempts to find the transition state shown in Figure 7 as $\mathbf{TS_{D12}}^-$ failed; a relaxed potential energy scan shows a very flat surface between **D1**$^-$ and **D2**$^-$. Formation of **D1**$^-$ from **D0**$^-$ and ethylene is much more favorable that the formation of **4** from **1** and ethylene because the latter involves significant orbital rearrangements that are assisted by the addition of **1**$^-$ to **1** in **D0**$^-$. Likewise, when these orbital rearrangements are subsequently dominated by the formation of ethylene bridge across the Ni−S bond in


dx.doi.org/10.1021/ic302236u | Inorg. Chem. 2013, 52, 3711−3723

**D2**$^-$, the strong binding of **1**$^-$ to the adduct is lost and **5** is released.

Computational studies have thus provided strong evidence for the involvement of dimetallic species in the mechanism leading to stable interligand adducts. This is a significant finding, and the question arises of whether experimental evidence can be obtained to further strengthen the evidence for dimetallic species. To this end, we performed mass spectrometry (ESI-MS, negative ion mode) in acetonitrile on an equimolar mixture of **1** and **1**$^-$ $NEt_4^+$. A signal centered at $m/z$ = 1151.8 corresponds to $[(Ni(tfd)_2)_2NEt_4]^-$. While this particular aggregate may be held together by pure electrostatics (through the $NEt_4^+$ apparently attracting two metal complex anions), a small signal with expected isotope signature indicative of the acetonitrile adduct of **D0**$^-$ ($C_{18}H_3F_{24}N_1Ni_2S_8^-$) was also seen (Supporting Information). This may be a close analogue of **D1**$^-$ or **D2**$^-$ where acetonitrile instead of ethylene is bound. Regarding the actual species **D1**$^-$ or **D2**$^-$, we think that the very flat energy landscape found in computations would make it very challenging to obtain direct experimental evidence for **D1**$^-$ or **D2**$^-$. However, for a charge-neutral association complex isomeric to but structurally distinctly different from **D1**$^-$ or **D2**$^-$, we have been able to obtain crystallographic information, as will be detailed below.

**Experimental Structure of a Dimetallic Complex Derived from Ethylene and 2 equiv of Ni(tfd)$_2$.** We had previously observed, using NMR spectroscopy on concentrated (on the order of 30 mM) solutions (Supporting Information to ref 15), that charge-neutral **1** reversibly associates with the ethylene adduct **2** to form an association complex of unknown structure. This dimetallic complex is labeled species "**D3**" in the following. Apart from dissociation, the association complex is unreactive and does not transform into any other species. In the kinetic studies (which were done using *n*-hexene), the relatively low concentrations of **1** and **2′**, along with the small equilibrium constant for association, led to a situation where formation of the association complex **D3′** does not need to be included in the kinetic treatment. While the association observed is unproductive and irrelevant under normal (dilute) kinetic conditions, this association is an interesting reaction, in particular given the computational evidence that other dimetallic complexes can be very reactive and mechanistically important. While bis(dithiolene) complexes of iron or cobalt frequently associate,[28] association is much rarer for nickel bis(dithiolene) complexes.[29] Heteroassociation between a nickel bis(dithiolene) complex and its alkene adduct was not known before our work. A more detailed look at such a heteroadduct is thus worthwhile. The association is best seen for the ethylene adduct. Formation of the association complex is reversible. The equilibrium constant for **1** + **2** ⇄ **D3** (at 293 K) was measured to be $K$ = 0.1 mM$^{-1}$, such that $\Delta G_{association}$ = −2.7 kcal mol$^{-1}$ at 293 K. Because of the relatively broad signals in the $^1$H NMR spectrum, no direct structural information was available, and the possibility that the ethylene bridge connects the two metal complex fragments in the dinuclear complex was tentatively suggested in 2006. We have in the meantime, from a concentrated solution of **1** and **2**, obtained crystals of dimetallic complex **D3**, in the form of a cocrystallizate with **1**. This new structure (sulfur-bridged, albeit in a rather unusual fashion) is disclosed here and sheds new light on the ability of nickel dithiolene complexes to form dimetallic species in the presence of alkenes.

Key crystallographic data are summarized in Table 2, and a view of the unit cell is shown in Figure 9. The unit cell contains

**Table 2. Crystallographic Data for D3$_2$·1**

| | |
|---|---|
| empirical formula | $C_{44}H_8F_{60}Ni_5S_{20}$ |
| formula weight | 2611.25 |
| temperature | 150(1) K |
| crystal system | monoclinic |
| space group | $P2_1/c$ |
| $a$ (Å) | 14.6053(4) |
| $b$ (Å) | 12.3214(5) |
| $c$ (Å) | 21.4161(7) |
| $\beta$ (deg) | 92.8830(2) |
| $V$ (Å$^3$) | 3849.1(2) |
| $Z$ | 2 |
| $d_{calcd}$ (g/cm$^3$) | 2.253 |
| $\theta$ range for data collection (deg) | 2.79−27.50 |
| reflns collected | 26 282 |
| independent reflns | 8756 |
| data/restraints/parameters | 8756/0/639 |
| GOF on $F^2$ | 1.007 |
| R1 ($I > 2\sigma(I)$)/wR2 (all data) | 0.0524/0.1385 |

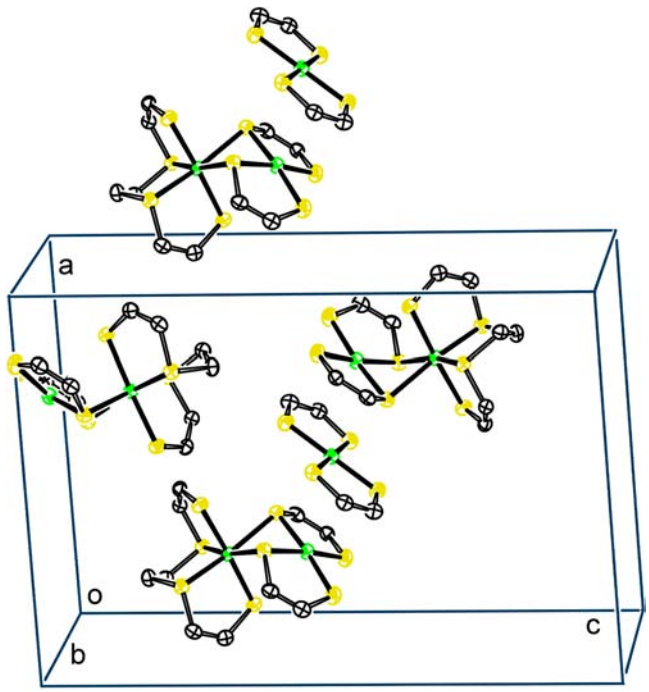


**Figure 9.** Packing of dinuclear complex **D3** and mononuclear reactant complex **1** (all trifluoromethyl groups omitted, for clarity) in the cocrystal **D3$_2$·1**.

two molecules of **D3** per one molecule of **1**. The molecule of **1** resides on crystallographic center of inversion while the molecule of **D3** resides on a general position. While **D3** is a dimetallic species already, cocrystallization with monometallic **1** did not lead to further aggregation: there are no close (smaller than van-der-Waals radii) contacts between **D3** and **1** in the crystal. The fact that the crystal of **D3** contains species **1** as a cocrystallizate leads to some potential ambiguity in the assignment of charges, since species **1** is very oxidizing and the possibility that it exists in one of its two reduced forms


dx.doi.org/10.1021/ic302236u | Inorg. Chem. 2013, 52, 3711−3723

(monoanionic or dianionic) in the crystal, with the other component oxidized, cannot be ruled out a priori. Since the composition is "$D3_2 \cdot 1$", the charge distribution could be either $(D3^0)_2(1^0)$ (*charge-neutral D3*) or $(D3^{0.5+})_2(1^-)$ (*half-electron-oxidized D3*, somewhat unlikely but not impossible in a solid state structure) or $(D3^+)_2(1^{2-})$ (*one-electron-oxidized D3*). Structural data suggest an assignment: one-electron reduction of a charge-neutral metal bis(dithiolene) complex of a nickel triad metal leads to shortening of the intraring C−C bonds (more double-bond character, toward enedithiolate ligand) and the trend continues when the dianion is formed by further reduction. During such reduction, while the C−C bonds contract, the S−C bonds elongate. Relevant intraring C−C bond lengths for species **1** in the crystal (Table 3) are closer to

**Table 3. Intraring C−C and C−S Distances (Å) in the Molecular Structure of 1 in the Cocrystal $D3_2$·1, Compared to Literature Data for Ni(tfd)$^{0/1-}$ ($1^{0/1-}$) and Pt(tfd)$^{0/1-/2-}$[a]**

| | C−C (in ring) | C−S | ref | comment |
|---|---|---|---|---|
| | | no charge | | |
| **1** in $D3_2$·**1** | 1.378(7) | 1.702(5) | this work | suggested to be charge-neutral |
| | | 1.695(5) | | |
| **1** | 1.382(6) | 1.687(4)* | 25 | |
| $Pt(tfd)_2$ | 1.380(9) | 1.70(1)* | 10d | |
| | | reduced | | |
| $1^-$ | 1.348(15) | 1.73(1)* | 30 | $Cp_2Fe^+$ salt |
| $Pt(tfd)_2^-$ | 1.354(12) | 1.726(8)* | 31 | $AsPh_4^+$ salt |
| | | doubly reduced | | |
| $Pt(tfd)_2^{2-}$ | 1.348(9) | 1.75(1)* | 10e | $NEt_4^+$ salt |

[a]Structural data suggest that the cocrystal contains charge-neutral **1** and consequently charge-neutral **D3**. Comment: * indicates a C−S distance average of 2 values.

those observed for neutral **1** than literature data for $1^-$ (*longer* C−C bonds in **1** compared to $1^-$) although the difference is only 1.3 times the sum of the two standard deviations. However, another observation, with the same level of statistical significance, is independently made for the C−S distances (*shorter* C−S bonds in **1** compared to $1^-$), where neutral **1** is again indicated. Finally, comparison with literature data for the platinum analog with the same tfd ligand, namely, Pt(tfd)$^{0/1-/2-}$ (Table 3), is perfectly consistent. We conclude that we have fairly good structural support for an assignment stating that *charge-neutral D3* is present. The molecular structure of **D3** is shown in Figure 10.

The dimetallic structure contains one pseudo-square-planar nickel center and one pseudo-octahedral nickel center. The structure can be seen as arising from adding a bidentate chelate ligand, namely complex **1** with two *cis*-sulfurs on separate dithiolene ligands, to the nickel center of complex **2** such that the coordination number for **2** increases from 4 to 6. The fragment that arose from complex **2** (the fragment having the ethylene bridge) has rearranged such that the two thiolates that were initially in cis position have moved into mutually trans positions, opening up two cis sites where the fragment that stems from complex **1** is now chelating. Deviations from ideal angles (90° and 180°) are surprisingly small, smaller than 13° (legend to Figure 10). Consistent with the observed small driving force, the newly formed bonds seem fairly weak, judged by their lengths. The bonds between the two fragments, namely bond Ni2−S7 and bond Ni2−S10 are extremely long, at

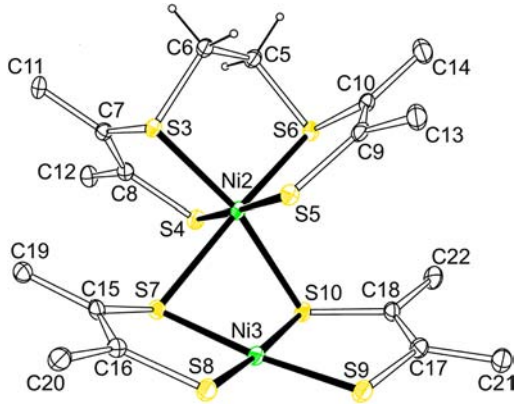


**Figure 10.** Structure of **D3** in the cocrystal $D3_2$·**1**, using 30% probability envelopes (fluorines omitted, for clarity; hydrogens as spheres of arbitrary radius). The molecule of **1**, not shown here, contains Ni1, S1, and S2. Selected distances and angles (Å, deg) for **D3**: (a) octahedral part involving Ni2 Ni2−S3, 2.2694(13); Ni2−S4, 2.2369(14); Ni2−S5, 2.2375(13); Ni2−S6, 2.2753(14); Ni2−S7, 2.4528(14); Ni2−S10, 2.3806(14); Ni2−Ni3, 2.9780(9); S3−C7, 1.773(5); S4−C8, 1.720(5); S5−C9, 1.739(5); S6−C10, 1.775(5); C7−C8, 1.353(7); C9−C10, 1.344(7); S4−Ni2−S5, 176.80(6); S4−Ni2−S3; 89.99(5); S4−Ni2−S6, 86.91(5); S3−Ni2−S6; 93.48(5); S3−Ni2−S10; 167.20(5); S6−Ni2−S10, 98.70(5); S4−Ni2−S7, 85.59(5); S5−Ni2−S7, 97.61(5); S6−Ni2−S7, 170.94(5); S10−Ni2−S7, 75.81(5); (b) square-planar part involving Ni3 Ni3−S7, 2.1426(14); Ni3−S8; 2.1401(15); Ni3−S9, 2.1383(15); Ni3−S10, 2.1560(15); S7−C15, 1.730(5); S8−C16, 1.706(5), S9−C17, 1.713(5); S10−C18, 1.740(5); C15−C16, 1.375(7); C17−C18, 1.369(7); S9−Ni3−S8, 86.89(6); S9−Ni3−S7, 172.82(6); S8−Ni3−S7, 92.29(5); S9−Ni3−S10, 92.44(6); S8−Ni3−S10, 172.21(6).

2.4528(14) and 2.3806(14) Å, respectively. This is even longer (by about 6%) than bonds between nickel and weakly coordinating thioether ligands (such as Ni2−S3/S6, see legend to Figure 10). It is surprising that a ligand as weakly donating as complex **1** can trigger complex **2** to switch from square-planar to octahedral. We have contemplated the question of whether intramolecular electron transfer has occurred between the two fragments within dinuclear **D3**, such that the fragment arising from complex **1** is reduced and the octahedral nickel complex oxidized ($Ni^{III}$ or $Ni^{IV}$). Crystallographic bond lengths contain too much uncertainty to clearly confirm or refute this hypothesis. The intraring C−C distances as long as C−S distances within the dithiolene moiety of the square-planar fragment (C15−C16, 1.375(7); C17−C18, 1.369(7) ; S8−C16, 1.706(5); S9−C17, 1.713(5)) are in fact more consistent with a neutral fragment (Table 3) and less consistent with a reduced fragment. Crystallographic data thus point toward coordination with rearrangement (square planar → octahedral) but without electron transfer, although the crystallographic evidence against intramolecular electron transfer is somewhat weak, given the standard deviations. Gratifyingly, providing additional confirmation that the computational method used is very appropriate, **D3** is computed to be a stable species (local minimum). A geometry optimization with octahedral $Ni^{IV}$ and square-planar $Ni^{II}$ yields structural parameters for the computed structure (Figure 11) that are very similar to those of the experimental structure (Figure 10), again suggesting that the computational method used is suitable. Resonance structures with charge-separated fragments (octahedral $Ni^{IV}$ and square-planar $Ni^{II}$) and neutral fragments (octahedral $Ni^{II}$ and square-planar $Ni^{II}$) for dinuclear **D3** could be drawn, as shown in


dx.doi.org/10.1021/ic302236u | *Inorg. Chem.* 2013, 52, 3711−3723

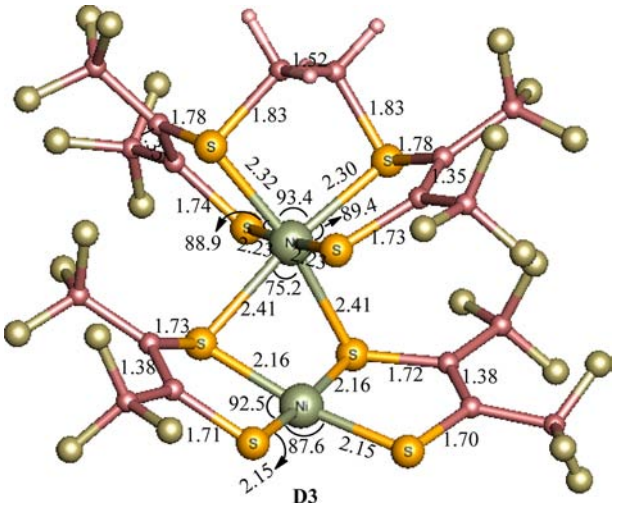


**Figure 11.** Calculated geometry of **D3** with selected distances (Å) and angles (deg).

Figure 12. Charge distribution calculation from AIM[32,33] shows that there is 0.23 of an electron charge transferred from the

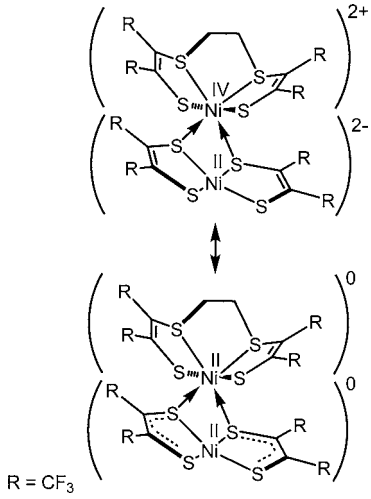


**Figure 12.** Resonance structures for dinuclear **D3**.

octahedral fragment to the square-planar fragment, suggesting a significant but not overwhelming contribution from the upper resonance structure in Figure 12 to dinuclear **D3** (of course, many additional resonance structures would be needed for a complete description).

We can conclude here that while square-planar dithiolenes acting as ligands have been observed previously,[34] the structure of **D3** is rather unique: first, it is rare that charge-neutral dithiolene complexes are employed as ligands (it is more common that the reduced forms are used as ligands), second it is quite unexpected that this donation leads to a rapid and reversible (in solution) switch between square planar and octahedral in the complex which the dithiolene donates to. Complex **D3** is isomeric (except for the charge) to the dimetallic species $\mathbf{D1}^-$ and $\mathbf{D2}^-$ that play a key role, according to our computations, in the alkene binding mechanism. **D3** is a constitutional isomer of these key species and thus in terms of bonding involved quite different from the dimetallic species that lie on the reaction pathway for interligand alkene binding. Still, the experimental results for **D3** impressively demonstrate the facility of association and structural reorganization for a dinuclear system containing two nickel bis(dithiolene) complexes and one alkene. This initially very surprising structure is very well reproduced with the DFT methods used, confirming the validity of the method for dinuclear dithiolene complexes of nickel.

## CONCLUSION

In conclusion, a computational study, aided by experimental kinetics, has elucidated the mechanism for the unconventional (ligand-based) reaction between alkenes and $Ni(tfd)_2$ (**1**). In experiment, intraligand adduct followed by decomposition is observed with pure $Ni(tfd)_2$ and ethylene, while catalytic amounts of $[Ni(tfd)_2]^-$ ($\mathbf{1}^-$) lead to a change in selectivity. Computations show that the intrinsic reactivity of $Ni(tfd)_2$ (in the absence of $[Ni(tfd)_2]^-$) favors the unstable intraligand adduct, which is formed in a symmetry-allowed reaction. A $[Ni(tfd)_2]^-$ anion catalyzes formation of the stable interligand adduct, while simultaneously reducing the rate of formation of the intraligand adduct. The intimate mechanism of these steps remained puzzling, but the computational results of this study have provided a very satisfactory solution: the reduced complex $\mathbf{1}^-$ reacts with **1** to form a stable dimetallic intermediate. Ethylene rapidly binds to this intermediate. Isomerization to form a complex in which ethylene is bound across the Ni–S bond is facile, and also $\mathbf{1}^-$ is then released easily. The short-lived Ni–S alkene adduct isomerizes rapidly, notably much more rapidly to the (stable) interligand adduct than to the (unstable) intraligand adduct. In terms of computed overall free energy of activation, this anion-catalyzed reaction competes effectively and suppresses the formation/decomposition of intraligand adducts (which would be formed in the absence of the anion) as shown in Scheme 7. The discovery of the effect of

**Scheme 7**

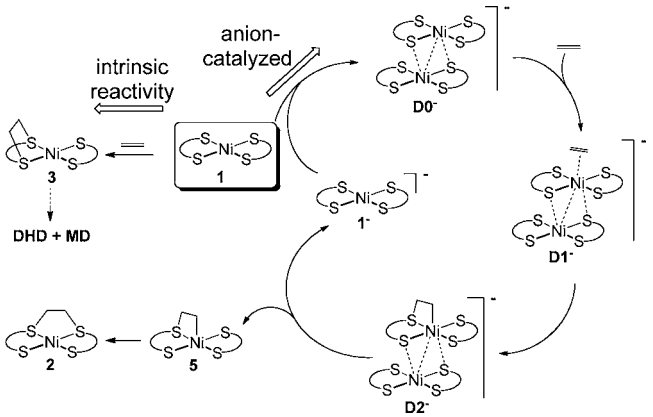


the reduced (anionic) nickel complex on product selectivity[15] raised intriguing mechanistic questions, answered in the present contribution. Computations strongly indicate the key involvement of dimetallic complexes, formed from two nickel bis(dithiolene) complexes and one alkene, that are anionic. A structurally distinct charge-neutral dimetallic species has been experimentally characterized. Although it is not an intermediate on the reaction pathway, it demonstrates the feasibility of aggregates from two nickel bis(dithiolene) complexes and one alkene. Given the recent interest in ligand-based alkene reactions, we think the current analysis of the prototypical $Ni(tfd)_2$ reactivity will aid in future work in this area.


dx.doi.org/10.1021/ic302236u | Inorg. Chem. 2013, 52, 3711–3723

## METHODS

Preliminary examination of the simplified dithiolene $Ni(S_2C_2H_2)_2$[35] shows that calculations with the $\omega$B97X-D[36] functional, which contains both long-range exchange and empirical dispersion corrections that are very important for the modeling processes with weak interactions and localized anionic or strongly electron donating sites, produced relative electronic energies that were similar to CCSD[37] results. Therefore, this functional was applied to the calculation of the mechanism of the reactions of $Ni(S_2C_2(R)_2)_2^{0/1-}$ (R = $CF_3$) with ethylene describe here, M06[38] was also used to do the single point calculation based on the $\omega$B97X-D optimized geometry (Supporting Information). All calculations were performed using Gaussian 09[39] and an all-electron 6-31++G** Pople basis set[40] was specified for H, C, F, S, and Ni atoms, this specification uses the Wachters–Hay basis set for Ni.[41] The geometric structures of all species were optimized at gas-phase. Calculating the harmonic vibrational frequencies and noting the number of imaginary frequencies confirmed the nature of all intermediates (no imaginary frequency) and transition states (only one imaginary frequency). The transition states were also confirmed to connect appropriate intermediates, reactants, or products by intrinsic reaction coordinate (IRC) calculations,[42] however, a scan of the geometric changes between the two intermediates, $\mathbf{D1}^-$ and $\mathbf{D2}^-$, revealed a transition state very close to $\mathbf{D2}^-$, but we were unable to characterize this transition state further. How this issue affects our results is described in the caption to Figure 7, which shows the energy diagram for these reaction coordinates. The gas-phase free energies for all species, *G*, were calculated at *T* = 298.15 K within the harmonic potential approximation at optimized structures. The solvation effects with chloroform as solvent were simulated by the SMD solvent model[43] based on the gas phase optimized geometries. We calculate the solution phase free energy by adding solvation energies on the gas phase relative free energies. The solution phase free energies will be used in the discussions, unless otherwise specified. The 3D molecular structures displayed in the Supporting Information were drawn by using the JIMP2 molecular visualizing and manipulating program.[44] Experimental details, for kinetics as well as for crystallography on $\mathbf{D3}_2\cdot\mathbf{1}$, are given in the Supporting Information.

## ASSOCIATED CONTENT

### Supporting Information

Complete ref 39, figures of optimized compounds/intermediates and transition states, Dynafit script and raw kinetic data, along with analysis of fitting results (PDF), and crystallographic data for $\mathbf{D3}_2\cdot\mathbf{1}$ (CIF). This material is available free of charge via the Internet at http://pubs.acs.org.

## AUTHOR INFORMATION


### Corresponding Author

*E-mail: ulrich.fekl@utoronto.ca (U.F.); edward.brothers@qatar.tamu.edu (E.N.B.); hall@mail.chem.tamu.edu (M.B.H.).

### Present Addresses

[‖]Department of Chemistry, Faculty of Science, Cairo University, Giza, Egypt

[¶]Molecular Graphics and Computational Facility, College of Chemistry, University of California, Berkeley, CA, USA


### Notes

The authors declare no competing financial interest.

## ACKNOWLEDGMENTS

Funding by the Natural Science and Engineering Research Council (NSERC) of Canada (U.F.) is gratefully acknowledged. A.A. is a recipient of a University of Toronto Excellence Award. E.N.B. and M.B.H. acknowledge support from the Qatar National Research Fund under NPRP 08-426-1-074. We thank Dr. Peter Mitrakos and Mr. Neilson Nguyen (University of Toronto) for assistance with ESI-MS.

## REFERENCES


(1) (a) National Research Council. *Separation and Purification: Critical Needs and Opportunities*; National Academy Press: Washington, DC, 1987. (b) Blytas, G. C. In *Separation and Purification Technology*; Li, N. N., Calo, J. M., Eds.; Marcel Dekker: New York, 1992.

(2) Grantom, R. L.; Royer, D. J. In *Ullmann's Encyclopedia of Industrial Chemistry* 5th ed.; VCH: New York, 1987; pp 45–93.

(3) Suzuki, T.; Nobel, R. D.; Koval, C. A. *Inorg. Chem.* **1997**, *36*, 136.

(4) (a) Clark, G. R.; Waters, J. M.; Whittle, K. R. *J. Chem. Soc., Dalton Trans.* **1973**, 821. (b) Kajitani, M.; Kohara, M.; Kitayama, T.; Asano, Y.; Sugimori, A. *Chem. Lett.* **1986**, 2109. (c) Kajitani, M.; Kohara, M.; Kitayama, T.; Akiyama, T.; Sugimori, A. *J. Phys. Org. Chem.* **1989**, *2*, 131. (d) Kunkely, H.; Vogler, A. *Inorg. Chim. Acta* **2001**, *319*, 183. (e) Geiger, W. E. *Inorg. Chem.* **2002**, *41*, 136.

(5) (a) Schrauzer, G. N.; Mayweg, V. P. *J. Am. Chem. Soc.* **1965**, *87*, 1483. (b) Schrauzer, G. N.; Rabinowitz, H. N. *J. Am. Chem. Soc.* **1968**, *90*, 4297. (c) Schrauzer, G. N.; Ho, R. K. Y.; Murillo, R. P. *J. Am. Chem. Soc.* **1970**, *92*, 3508. (d) Zhang, C. H.; Reddy, K.; Chadha, R. K.; Schrauzer, G. N. *J. Coord. Chem.* **1992**, *26*, 117.

(6) (a) Schmitt, R. D.; Wing, R. M.; Maki, A. H. *J. Am. Chem. Soc.* **1969**, *91*, 4394. (b) Wing, R. M.; Tustin, G. C.; Okamura, W. H. *J. Am. Chem. Soc.* **1970**, *92*, 1935. (c) Baker, J. R.; Hermann, A.; Wing, R. M. *J. Am. Chem. Soc.* **1971**, *93*, 6486. (d) Herman, A.; Wing, R. M. *J. Organomet. Chem.* **1973**, *63*, 441.

(7) Wang, K.; Stiefel, E. I. *Science* **2001**, *291*, 106.

(8) Fan, Y.; Hall, M. B. *J. Am. Chem. Soc.* **2002**, *124*, 12076.

(9) (a) Petrenko, T.; Ray, K.; Wieghardt, K. E.; Neese, F. *J. Am. Chem. Soc.* **2006**, *128*, 4422. (b) Serrano-Andrés, L.; Avramopoulos, A.; Li, J.; Labéguerie, P.; Bégué, D.; Kello, V.; Papadopoulos, M. G. *J. Chem. Phys.* **2009**, *131*, 134312. (c) Bégué, D.; Labéguerie, P.; Zhang-Negrerie, D. Y.; Avramopoulos, A.; Serrano-Andrés, L.; Papadopoulos, M. G. *Phys. Chem. Chem. Phys.* **2010**, *12*, 13746.

(10) (a) Nomura, M.; Takayama, C.; Kajitani, M. *Inorg. Chem.* **2003**, *42*, 6441. (b) Szilagyi, R. K.; Lim, B. S.; Glaser, T.; Holm, R. H.; Hedman, B.; Hodgson, K. O.; Solomon, E. I. *J. Am. Chem. Soc.* **2003**, *125*, 9158. (c) Waters, T.; Woo, H.; Wang, X.; Wang, L. *J. Am. Chem. Soc.* **2006**, *128*, 4282. (d) Kogut, E.; Tang, J. A.; Lough, A. J.; Widdifield, C. M.; Schurko, R. W.; Fekl, U. *Inorg. Chem.* **2006**, *45*, 8850. (e) Tang, J. A.; Kogut, E.; Norton, D.; Lough, A. J.; McGarvey, B. R.; Fekl, U.; Schurko, R. W. *J. Phys. Chem. B* **2009**, *113*, 3298.

(11) A creative extension of the ligand-based alkene binding concept has led to highly reversible alkene binding to P,S-ligands: (a) Grapperhaus, C. A.; Ouch, K.; Mashuta, M. S. *J. Am. Chem. Soc.* **2009**, *131*, 64. (b) Ouch, K.; Mashuta, M. S.; Grapperhaus, C. A. *Inorg. Chem.* **2011**, *50*, 9904.

(12) (a) Harrison, D. J.; Lough, A. J.; Nguyen, N.; Fekl, U. *Angew. Chem., Int. Ed.* **2007**, *46*, 7644. (b) Harrison, D. J.; Fekl, U. *Chem. Commun.* **2009**, 7572.

(13) Kerr, M. J.; Harrison, D. J.; Lough, A. J.; Fekl, U. *Inorg. Chem.* **2009**, *48*, 9043.

(14) (a) Sun, L. L.; Zhang, S. F.; Han, Q. Z.; Zhao, Y. H.; Wen, H. *Acta Phys.-Chim. Sin.* **2010**, *26*, 3345. (b) Sun, L. L.; Zhang, S. F.; Han, Q. Z.; Zhao, Y. H.; Wen, H. *Mol. Simul.* **2011**, *37*, 813.

(15) Harrison, D. J.; Nguyen, N.; Lough, A. L.; Fekl, U. *J. Am. Chem. Soc.* **2006**, *128*, 11026.

(16) For a preliminary report, see: Dang, L.; Shibl, M. F.; Yang, X.; Alak, A.; Harrison, D. J.; Fekl, U.; Brothers, E. N.; Hall, M. B. *J. Am. Chem. Soc.* **2012**, *134*, 4481. New data not reported in that communication but reported here are the "monometallic, anionic" pathway (Figures 4 and 5) and everything involving the structure of **D3** as determined by X-ray crystallography and computations (Figures 9–12), whereas the introduction section and the mechanism involving $\mathbf{1}^-/\mathbf{D_0}^-$ contain previously reported work in a modified presentation (much extended discussion).

(17) When **DHD′** is produced, corresponding amounts of metal decomposition products (**MD**) are also formed, evidenced by numerous, overlapping $^{19}$F NMR peaks for oligomeric $[Ni(tfd)]_x$.
(18) Two diastereomers both of which are, in time traces, collectively reported as "species **2′**".
(19) Kuzmič, P. *Anal. Biochem.* **1996**, *237*, 260.
(20) A small systematic discrepancy is visible at early reaction times. For those data that involve a high concentration of $\mathbf{1}^-$, a reduced initial rate (induction period) for formation of **DHD′** is observed, an effect that is underestimated by the model. The model chosen *does* allow for an induction period for **DHD′**-production (**DHD′** is "stored" in the form of $\mathbf{3}'/\mathbf{3}'^+$ before it is liberated as free **DHD′**) but the fit to the model does not fully show the magnitude of the effect. We suggest that the more pronounced induction period in the experimental data compared to the model likely stems from small concentrations of **DHD′** being underestimated due to line broadening in the sample because the samples becomes more paramagnetic for higher $\mathbf{1}^-$ concentrations. A tighter fit to the experimental curves is, of course, obtained if those curves are fit individually. The globally best parameters, however, are the parameters not from local optimization but from global optimization, and this is the method chosen and shown in Figure 1.
(21) Burnham, K. P.; Anderson, D. R. *Model Selection and Multimodel Inference*, 2nd ed.; Springer: New York, 2002.
(22) Miller, T. R.; Dance, I. G. *J. Am. Chem. Soc.* **1973**, *95*, 6970.
(23) Cusumano, M.; Ricevuto, V. *J. Chem. Soc., Dalton Trans.* **1978**, 1682.
(24) Making this step only second order degrades the quality of the fit.
(25) Wang, K.; Patil, A. O.; Zushma, S.; McConnachie, J. M. *J. Inorg. Biochem.* **2007**, *101*, 1883.
(26) Shibl, M. F.; Dang, L.; Raju, R. K.; Hall, M. B.; Brothers, E. N. *Int. J. Quantum Chem.* **2012**, DOI: 10.1002/qua.24370.
(27) Szilagyi, R. K.; Lim, B. S.; Glaser, T.; Holm, R. H.; Hedman, B.; Hodgson, K. O.; Solomon, E. I. *J. Am. Chem. Soc.* **2003**, *125*, 9158.
(28) (a) Balch, A. L.; Dance, I. G.; Holm, R. H. *J. Am. Chem. Soc.* **1968**, *90*, 1139. (b) Jacobsen, H.; Donahue, J. P. *Inorg. Chem.* **2008**, *47*, 10037.
(29) Geiger, W. E; Barrière, F.; LeSuer, R. J.; Trupia, S. *Inorg. Chem.* **2001**, *40*, 2472.
(30) Miller, J. S.; Calabrese, J. C.; Epstein, A. J. *Inorg. Chem.* **1989**, *28*, 4230.
(31) Hosking, S.; Lough, A. J.; Fekl, U. *Acta Crystallogr.* **2009**, *E65*, m759−m760.
(32) Bader, R. F. W. *Atoms in Molecules. A Quantum Theory*; Oxford: Clarendon Press, 1990.
(33) Keith, T. A. *AIMAll*, version 12.06.03; TK Gristmill Software: Overland Park KS, U.S.A., 2012.
(34) (a) Harrison, D. J.; De Crisci, A. G.; Lough, A. J.; Kerr, M. J.; Fekl, U. *Inorg. Chem.* **2008**, *47*, 10199. (b) Maiti, B. K.; Pal, K.; Sarkar, S. *Dalton Trans.* **2008**, 1003. (c) Adams, H.; Gardner, H. C.; McRoy, R. A.; Morris, M. J.; Motley, J. C.; Torker, S. *Inorg. Chem.* **2006**, *45*, 10967. (d) McLauchlan, C. C.; Ibers, J. A. *Inorg. Chem.* **2001**, *40*, 1809. (e) Breitzer, J. G.; Rauchfuss, T. B. *Polyhedron* **2000**, *19*, 1283. (f) Roesselet, K.; Doan, K. E.; Johnson, S. D.; Nicholls, P.; Miessler, G. L.; Kroeker, R.; Wheeler, S. H. *Organometallics* **1987**, *6*, 480.
(35) Dang, L.; Yang, X.; Brothers, E. N.; Hall, M. B. *J. Phys. Chem. A* **2012**, *116*, 476.
(36) Chai, J. D.; Head-Gordon, M. *Phys. Chem. Chem. Phys.* **2008**, *10*, 6615.
(37) (a) Cizek, J. In *Advances in Chemical Physics*, Vol. *14*; Hariharan, P. C., Ed.; Wiley Interscience: New York, 1969; p 35. (b) Purvis, G. D., III; Bartlett, R. J. *J. Chem. Phys.* **1982**, *76*, 1910. (c) Scuseria, G. E.; Janssen, C. L.; Schaefer, H. F., III *J. Chem. Phys.* **1988**, *89*, 7382. (d) Scuseria, G. E.; Schaefer, H. F., III *J. Chem. Phys.* **1989**, *90*, 3700.
(38) Zhao, Y.; Truhlar, D. G. *Theor. Chem. Acc.* **2008**, *120*, 215.
(39) Frisch, M. J. et al. *Gaussian 09*; Gaussian, Inc., Wallingford CT, 2009.
(40) Krishnan, R.; Binkley, J. S.; Seeger, R.; Pople, J. A. *J. Chem. Phys.* **1980**, *72*, 650.
(41) (a) Wachters, A. J. H. *J. Chem. Phys.* **1970**, *52*, 1033. (b) Hay, P. J. *J. Chem. Phys.* **1977**, *66*, 4377.
(42) (a) Fukui, K. *J. Phys. Chem.* **1970**, *74*, 4161. (b) Fukui, K. *Acc. Chem. Res.* **1981**, *14*, 363.
(43) Marenich, A. V.; Cramer, C. J.; Truhlar, D. G. *J. Phys. Chem. B* **2009**, *113*, 6378.
(44) (a) Manson, J.; Webster, C. E.; Hall, M. B. *JIMP2, A Free Program for Visualizing and Manipulating Molecules*, version 0.091; Texas A&M University: College Station, TX, 2006. (b) Hall, M. B.; Fenske, R. F. *Inorg. Chem.* **1972**, *11*, 768.